P H Y S I C A L   R E V I E W   L E T T E R S

Physical Origins of the New Magnetoresistance in Pt/YIG

B. F. Miao,[1,2] S. Y. Huang,[1] D. Qu,[1] and C. L. Chien[1,*]

[1]*Department of Physics and Astronomy, Johns Hopkins University, Baltimore, Maryland 21218, USA*
[2]*National Laboratory of Solid State Microstructures and Department of Physics,*
Nanjing University, Nanjing 210093, People's Republic of China

A new type of magnetoresistance (MR) observed in Pt/YIG when nominally nonmagnetic Pt comes in contact with a ferrimagnetic insulator yttrium iron garnet (YIG) has drawn intense experimental and theoretical interest. In this Letter, we experimentally demonstrate two physical origins of the new MR: a spin current across the Pt/YIG interface and the magnetic proximity effect. The new MR can also be reproduced when Pt is in contact with a nonmagnetic insulator doped with a few percent of Fe impurities. By tuning the YIG surface and inserting an Au layer between the Pt and YIG, we are able to separate the two contributions.

After spectacular advances and successes of metal-based spintronic phenomena and devices, insulator-based spintronics has attracted a lot of attention, including spin pumping [1], magnonics [2], and the spin Seebeck effect (SSE) [3]. In many cases, it involves $Y_5Fe_3O_{12}$ (YIG) as the magnetic insulator and Pt as the spin current detector. Recently, a new type of magnetoresistance (MR) in a Pt/YIG hybrid structure was discovered [4–10]. As a nonmagnetic metal, Pt in isolation shows no discernible MR. In contrast, a thin Pt layer in contact with a ferrimagnetic insulator YIG exhibits a sizable MR whose magnitude decreases with increasing Pt thickness [5,7]. The MR in Pt/YIG depends on the direction of the magnetization (M) of the underlying YIG with respect to the current. The MR behavior of Pt/YIG with an in-plane field is $R_{||} > R_T$ [4–6], which is identical to the well-known anisotropic MR (AMR) in most ferromagnetic metals [11,12], where $R_{||}$ and R_T are the longitudinal ($M||I$) and transverse ($M \perp I$ and M oriented in the film plane) MR, respectively. However, the key difference lies in $R_\perp$ (perpendicular MR, $M \perp I$, and M oriented perpendicularly to the film plane), which can be accessed by a perpendicular magnetic field overcoming the demagnetizing field of the ferromagnet [6–8]. The unique characteristics of the new MR, as revealed at room temperature, that differ from those of all other known MRs including AMR are

$$R_{||} > R_T \approx R_\perp \quad \text{in AMR,} \tag{1}$$

$$R_\perp \approx R_{||} > R_T \quad \text{in the new MR}[6–8]. \tag{2}$$

Its simple form, as shown in Eq. (2), the mechanism of the new MR remains an outstanding problem.

The spin Hall MR (SMR) due to spin/charge current conversion [6,13] and the hybrid MR due to the magnetic

proximity effect (MPE) [7] have been proposed to account for the new MR. The SMR model in which Pt remains nonmagnetic involves the conversion of the charge/spin current propagating in the Pt layer due to the spin Hall effect (SHE), the inverse spin Hall effect (ISHE), and the concurrent absorption and reflection of the spin current at the surface of the ferromagnetic insulator [6,13]. In contrast, the hybrid MR draws from ample evidence of the induced Pt moment including MR [7], the anomalous Hall effect (AHE) [5], spin pumping [14], and x-ray magnetic circular dichroism (XMCD) [15] as well as theoretical calculations [16]. However, the nature of the intriguing new MR remains to be resolved.

In this Letter, by investigating the new MR in different systems and revealing its field dependence, we demonstrate that the new MR has two contributions from the spin current and MPE. Both contributions give the unique angular dependence of $R_\perp \approx R_{||} > R_T$. The MR at low field is mainly related to the spin current transmitted across the Pt/YIG interface, whereas at high field, it is due to the MPE. The contribution of the spin current decreases, while that of the MPE increases with increasing magnetic field H. By inserting an Au layer thicker than 6 nm between the Pt and YIG, the intrinsic spin current contribution can be isolated.

In addition to polycrystalline YIG (typically $6 \times 3 \times 0.5$ mm^3), we have used other specially treated substrates to bring out new aspects in MR. In one case, the YIG surface was purposely altered by Ar ion beam bombardment (500 V, current density 0.4 mA/cm^2) for 5 min. As a result, the electrical resistance of the altered YIG (noted as YIG$_{BB}$) decreases to about 4 MΩ from over 100 MΩ before the bombardment. The x-ray photoelectron spectroscopy confirms the existence of a metallic Fe state in the surface of YIG$_{BB}$. The altered YIG surface greatly reduces the spin-mixing conductance at the Pt/YIG interface [17],

thus, blocking the spin current transmission. In another case, in the place of YIG, a layer of 5-nm thick SiO_2 containing 7 at. % of Fe [SiO_2 (7% Fe)] was deposited by rf magnetron sputtering on the thermal oxidized Si (100) substrates. The Fe content is too low to be ferromagnetic, but it contains Fe granules with magnetic moments to simulate the MPE.

On top of these substrates, we deposited polycrystalline Pt thin films by dc magnetron sputtering and patterned these samples denoted as Pt/YIG, Pt/YIG_{BB}, and Pt/SiO_2 (7% Fe), into Hall bars of 0.2 mm in width with a long segment (5 mm) for the current and three short side bars 1.5 mm apart as voltage leads, as shown in Fig. 1(a). The thickness and structure have been measured by x-ray reflectivity and an x-ray diffractometer, respectively. The AFM measurements show that the surface roughness of YIG and SiO_2 (7% Fe) are around 0.3 nm. The xyz axes are parallel to the substrate edges with the x axis along the long segment of the Hall bar. In the MR measurements, the magnetic field (H) has been applied in the xy, xz, and yz planes with angles ϕ_{xy}, α_{xz}, and θ_{yz} relative to x, x, and z. Whereas the ϕ_{xy} scan accesses the longitudinal ($R_{\parallel}$) and the transverse (R_T) resistances with H parallel to the x and y axes, respectively, and the θ_{yz} scan and α_{xz} scan access the perpendicular resistance ($R_{\perp}$) with H along the z axis. By placing the samples between and in contact with two large Cu plates maintained at different constant temperatures, a perpendicular temperature gradient $\nabla_z T \approx 20$ K/mm can be established. The SSE in YIG drives a pure spin current flow along the z direction and can be detected as thermal voltage V_{th} via the ISHE with $E_{ISHE} \propto J_S \times \sigma$ in the Pt layer [3,18].

Figure 1(b) presents the field (H) dependence of the thermal voltage V_{th} for Pt(3 nm)/YIG, Pt(3 nm)/YIG_{BB}, and Pt(3 nm)/SiO_2 (7% Fe) with H along the y axis. The thermal voltage in Pt(3 nm)/YIG (black curve) with a magnitude of about 10 μV is asymmetric with H due to the spin current from the SSE in YIG. The small loop near the origin and the saturation field at about 500 Oe are the signature of the rectangular shape of the polycrystalline YIG substrate [5,18]. In contrast, the negligible V_{th} in

Pt(3 nm)/YIG_{BB} (red curve) and Pt(3 nm)/SiO_2 (7% Fe) (blue curve) shows that the spin current has been blocked by the altered YIG_{BB} surface, and it is absent in SiO_2 (7% Fe).

We show the field and angular dependence of the resistance and the AHE of Pt(3 nm)/YIG, Pt(3 nm)/YIG_{BB}, and Pt(3 nm)/SiO_2 (7% Fe) where the linear background due to the ordinary Hall effect (OHE) has been subtracted in the three columns of Fig. 2. The first row shows the well-known results for Pt(3 nm)/YIG with $R_{\parallel} > R_T$. Both the ϕ_{xy} scan and θ_{yz} scan have (cosine)^2 angular dependence, while the α_{xz} scan has no variation, i.e., the new MR described in Eq. (2) [7]. A recent theoretical model termed the spin Hall MR has been proposed to explain the new MR in the Pt/YIG hybrid structures [6,13]. It involves a successive conversion between the charge and spin current. A charge current in Pt generates a transverse spin current (spin index σ along the y axis) towards YIG due to the SHE, and that is either reflected ($M \| \sigma$) or absorbed ($M \perp \sigma$) at the Pt/YIG interface via the spin transfer torque. The reflected spin current, in turn, induces an additional charge current due to the ISHE in Pt. The combination of the spin transfer torque and ISHE gives rise to an angular dependence of (cosine)^2 as described by a double vector cross product [6,13]. The MR ratio in the SMR is proportional to θ_{SH}^2(Pt), where θ_{SH}(Pt) is the spin Hall angle. The resistance difference (e.g., $\Delta R = R_{\parallel} - R_T$) depends only on the relative angle between the spin index σ and the YIG magnetization M [6,13]. Therefore, according to the SMR model, ΔR should be a constant after YIG has been saturated by a small field of 2 kOe, provided that the magnetic field does not affect σ. However, this is not observed. Instead, as shown in Fig. 2(a), $\Delta R/R$ of Pt/YIG continues to increase nearly twice as large from 2.6×10^{-4} at 1 kOe to 4.5×10^{-4} at 80 kOe unabated. Similar behavior has also been observed on Pd/YIG recently [19].

On the other hand, Pt is near the Stoner ferromagnetic instability and exhibits induced moments when deposited on ferromagnetic metals, such as Fe [20], Co [21], Ni [22], and insulator YIG [15], as confirmed by XMCD. Evidence of the MPE in Pt has also been observed from transport measurements on ferromagnetic metals in addition to ferrimagnetic insulators [7]. Thus, we ascribe the MR at high field to the MPE when Pt is in contact with magnetic materials. Moreover, although no measurable MR can be observed for Pt(3 nm)/YIG_{BB} at low field where the spin current has been blocked, the new MR emerges at higher field, as shown in the middle row of Fig. 2(a). The value of $\Delta R/R$ increases from zero with increasing H and reaches 1.3×10^{-3} at 80 kOe. The sharp difference between the MR results of Pt/YIG and Pt/YIG_{BB} demonstrates that there are two contributions to the new MR: one correlates with the spin current transmission across the Pt/YIG interface that appears or disappears with the spin thermal
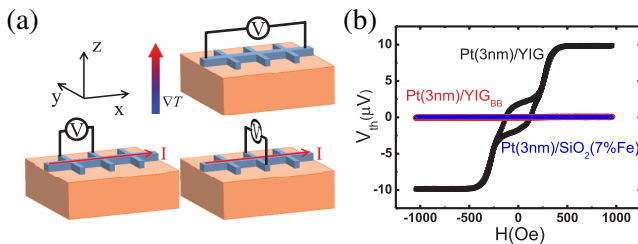
FIG. 1 (color online). (a) Schematics for the measurements of thermal voltage V_{th} with temperature gradient along the z axis, magnetoresistance, and anomalous Hall effect. (b) Field dependence of V_{th} for Pt(3 nm)/YIG, Pt(3 nm)/YIG_{BB} after ion bombardment for 5 min on YIG, and Pt(3 nm)/SiO_2 (7% Fe).
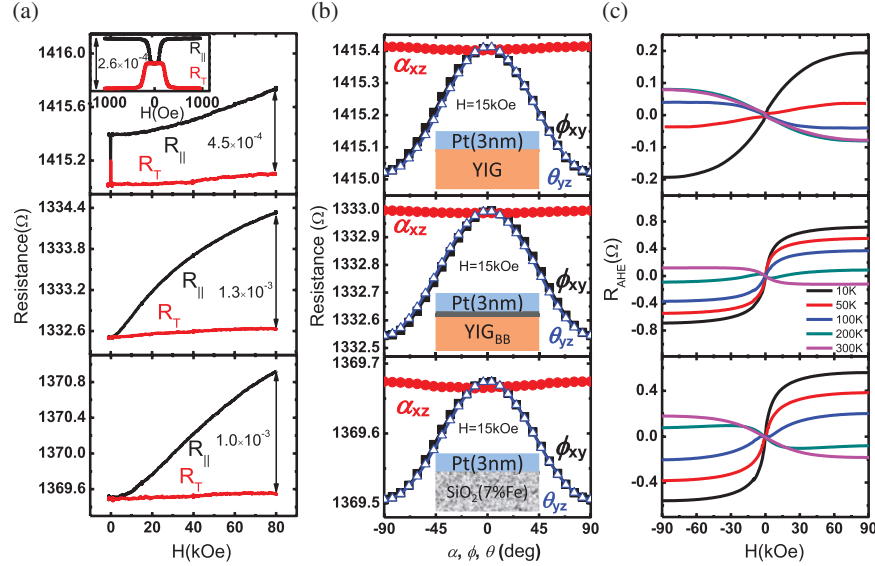
FIG. 2 (color online).   (a) Field dependence of longitudinal ($R_{\parallel}$) and transverse resistance (R_T), (b) angular dependence of the ϕ_{xy} scan, θ_{yz} scan, and α_{xz} scan, and (c) the field dependence of the anomalous Hall resistance at different temperatures of Pt(3 nm)/YIG (top row), Pt(3 nm)/YIG$_{BB}$ after ion bombardment for 5 min on YIG (middle row), and Pt(3 nm)/SiO$_2$ (7% Fe) (bottom row). The insert of (a) shows the H-dependent MR at low field (<1000 Oe) for Pt(3 nm)/YIG.

voltage simultaneously and the other is related to the MPE that dominates at H higher than about 3 kOe and continues to increase with H. Notably, both contributions of the new MR follow $R_{\perp} \approx R_{\parallel} > R_T$ and have the (cosine)^2 angular dependence for all the angular scans when H is sufficiently larger than the demagnetization field of YIG.

We next describe the results for Pt(3 nm)/SiO$_2$ (7% Fe) where SiO$_2$ (7% Fe) is not ferromagnetic but consists of Fe granules with magnetic moments and insulating. Interestingly, Pt(3 nm)/SiO$_2$ (7% Fe) exhibits very similar MR behavior to that of Pt/YIG$_{BB}$ at all fields: $\Delta R \approx 0$ at low field ($H < 1$ kOe), and $\Delta R/R$ increases to 1.0×10^{-3} at 80 kOe [Fig. 2(a)]. Equally interesting, the MR of Pt(3 nm)/SiO$_2$ (7% Fe) and Pt(3 nm)/YIG$_{BB}$ shows the same angular dependence as that of Pt(3 nm)/YIG. Both the ϕ_{xy} scan and θ_{yz} scan have (cosine)^2 angular dependence, while the α_{xz} scan has no variation, i.e., $R_{\perp} \approx R_{\parallel} > R_T$, the new MR. We note the (cosine)^2 dependence is a general consequence of anisotropic transport whenever a noncollinear electrical field E and current density j exist [12] and not exclusive to the mechanisms in the SMR model.

It is also revealing to compare the Hall results in Pt/YIG, Pt/YIG$_{BB}$, and Pt/SiO$_2$ (7% Fe). In addition to Pt/YIG, Pt/YIG$_{BB}$ also exhibits a pronounced AHE in Fig. 2(c). The AHE resistance R_{AHE} increases with deceasing temperature and even changes sign. Since the spin current across the Pt/YIG interface has been blocked by the altered YIG$_{BB}$ surface, the AHE should originate from the MPE. Concurrent with the new MR at high field, the AHE also emerges in Pt(3 nm)/SiO$_2$ (7% Fe), which contains no YIG. In this manner, we can artificially introduce the MPE, the associated new MR, and the AHE on Pt/SiO$_2$ (7% Fe). For comparison, Pt/SiO$_2$ shows no angular-dependent MR or AHE.

Recently, intrinsic SSE has been observed in Au/YIG free of the MPE without measurable MR or AHE [16]. Unlike Pt, which suffers from the MPE, Au is an intrinsic spin current detector endowed with a relatively long spin diffusion length [23]. Thus, if Au is inserted between Pt and YIG, the MPE is expected to decrease [24] but the intrinsic spin-related MR should remain. These expectations are born out in the temperature-dependent Hall resistance of Pt(3 nm)/Au(2 nm)/YIG shown in Fig. 3(a). A small and negative AHE that has been observed at 300 K increases with decreasing temperature, changes sign, and becomes more pronounced at 10 K. Even though the AHE is smaller than that of Pt(3 nm)/YIG, the 2-nm Au layer is not sufficient to eliminate the MPE. As a result, the MR ratio of Pt(3 nm)/Au(2 nm)/YIG still increases with H up to 100 kOe even after YIG has been saturated [Fig. 3(b)], similar to that of Pt/YIG. However, when the intervening Au layer has been increased to 6 nm, no AHE but only OHE can be detected within the temperature range of 10–300 K, as shown in Fig. 3(c) for Pt(3 nm)/Au(6 nm)/YIG. Equally important, its MR exhibits a totally different behavior. After the saturation of YIG, $\Delta R/R$ of Pt(3 nm)/Au(6 nm)/YIG decreases with H [Fig. 3(d)]. This is the intrinsic spin-current-related MR without the MPE.

The SMR model also predicts an anomalous Hall-like SMR contribution due to the imaginary part of the spin-mixing conductance, which scales as θ_{SH}^2(Pt) [9,13]. Thus, the AHE within the SMR model scales with $\Delta R/R$, both
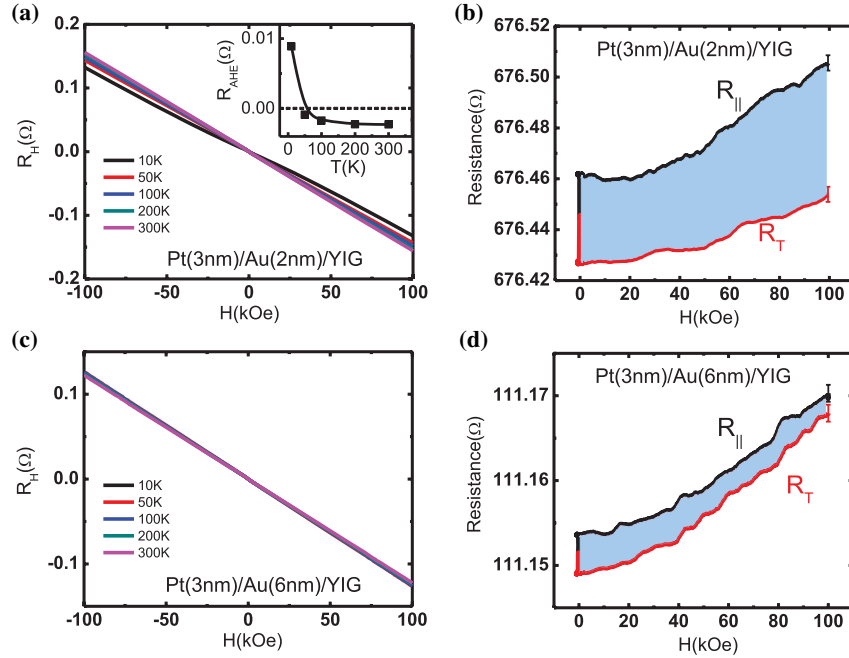
FIG. 3 (color online). Field dependence of the (a) Hall resistance R_H at different temperatures, (b) $R_\parallel$ and R_T for Pt(3 nm)/Au(2 nm)/YIG. Insert of (a) shows the temperature dependence of the anomalous Hall resistance R_{AHE} for Pt(3 nm)/Au(2 nm)/YIG. Field dependence of the (c) Hall resistance R_H at different temperatures, (d) $R_\parallel$ and R_T for Pt(3 nm)/Au(6 nm)/YIG.

proportional with $\theta_{SH}^2(Pt)$. Experimentally, Pt(3 nm)/Au(6 nm)/YIG and Pt(3 nm)/Au(2 nm)/YIG show a similar MR ratio at 1 kOe of 4.0×10^{-5} and 5.0×10^{-5}, respectively. On the contrary, no measurable AHE can be detected for Pt(3 nm)/Au(6 nm)/YIG. Therefore, the AHE is more likely due to the MPE instead of the spin current.

Figure 4(a) summarizes the H-dependent (from 1 to 80 kOe) $\Delta R/R$ for a series of Pt/Au(t)/YIG samples of different Au thicknesses. In Pt(3 nm)/Au(2 nm)/YIG (upper panel), the 2-nm Au layer is too thin to eliminate the MPE. As a result, $\Delta R/R$ of Pt(3 nm)/Au(2 nm)/YIG increases with increasing H, similar to that of Pt/YIG, even after YIG saturation. In contrast, no appreciable AHE can be detected in Pt(3 nm)/Au(6 nm)/YIG. Thus, the intrinsic spin current contribution to MR becomes dominant, and it decreases with increasing H (middle panel). Further increasing the thickness of Au to 10 nm gives similar results and with a faster decreasing rate. For Pt/YIG$_{BB}$, the spin transfer across the Pt/YIG interface has been blocked, and only the MPE remains. The MPE largely deceases after a thick Au layer (>6 nm) has been inserted between Pt and YIG. Thus, Pt(3 nm)/Au(10 nm)/YIG$_{BB}$ shows no measurable MR for the entire field range after the spin current and MPE are eliminated (lower panel). In this manner, we can tune the Pt/YIG interface to experimentally select the relative strength of spin-related MR or hybrid MR due to the MPE.

Figure 4(b) shows the Au thickness dependence of MR(t_{Au}) for Pt(3 nm)/Au(t)/YIG at 1 kOe. The value of $\Delta R/R$ decreases sharply after the insertion of 2 nm of Au and becomes roughly unchanged up to 10 nm of Au. Further increasing the Au layer thickness leads to a gradual decrease of $\Delta R/R$. Since Au/YIG has no measurable MR [16], the $\Delta R/R$ signal in Pt/Au/YIG is generated within the Pt layer only. However, the resistivity of Au is considerably lower than that of Pt, thus, shunting the MR signal in Pt. The AFM measurements show similar surface roughness of Au/YIG as those of YIG, YIG$_{BB}$, and SiO$_2$ (Fe). Considering a simple parallel resistor model, the resistance for the metal bilayer film Pt(3 nm)/Au(t_{Au}) is approximately $R_{Pt}R(t_{Au})/(R_{Pt} + R(t_{Au}))$, from which the MR within the Pt layer can be described as MR$_{int}(t_{Au}) = (1 + R_{Pt}/R(t_{Au}))$MR($t_{Au}$) [6], which evolves nonmonotonically with the Au thickness. The MR$_{int}(t_{Au})$ increases to 1.3×10^{-3} at 10 nm before decreasing at larger thickness [Fig. 4(c)]. A similar nonmonotonic behavior for the thermal voltage of Au/YIG has been observed [16], corroborating that the MR at low field is due to the spin current. The dashed line in Fig. 4(c) represents the $\Delta R/R$ for Pt(3 nm)/YIG, which is smaller than MR$_{int}(t_{Au})$ when $t_{Au} > 2$ nm. This suggests that inserting an Au layer may enhance the spin current transmission efficiency between Pt and YIG.

In summary, we experimentally demonstrate that the new MR in Pt/YIG has two physical origins. One is related to the spin current across the Pt/YIG interface. By inserting a thick Au layer (>6 nm) between Pt and YIG, we observe the intrinsic spin-current-related MR, where $\Delta R/R$ decays with increasing magnetic field H after YIG saturation. The
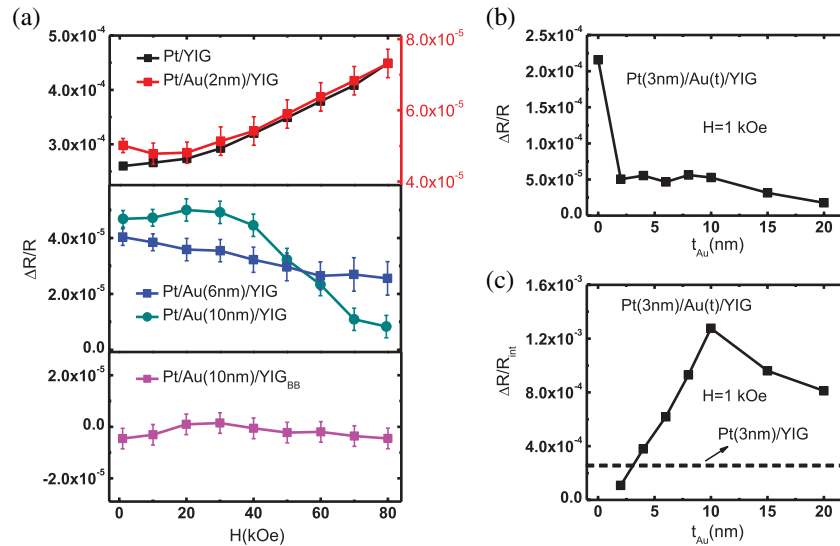
FIG. 4 (color online).   (a) Field dependence of MR ratio $\Delta R/R$ for upper panel Pt(3 nm)/YIG and Pt(3 nm)/Au(2 nm)/YIG, middle panel Pt(3 nm)/Au(6 nm)/YIG and Pt(3 nm)/Au(10 nm)/YIG, and lower panel Pt(3 nm)/Au(10 nm)/YIG$_{BB}$. (b) Au thickness dependence of $\Delta R/R$ for Pt(3 nm)/Au(t)/YIG at 1000 Oe. (c) The calculated intrinsic $\Delta R/R$ in Pt layer for Pt(3 nm)/Au(t)/YIG at 1000 Oe. Dashed line represents the result for Pt(3 nm)/YIG.

other is due to the MPE, which dominates at high field, and $\Delta R/R$ increases with increasing H. The effect of the MPE can be simulated in SiO_2 with the inclusion of Fe impurities. Furthermore, we find that the AHE in the Pt/YIG system as well as Pt/YIG$_{BB}$ and Pt/SiO$_2$ (7% Fe) is related to the MPE instead of the spin current. The nature of the new MR in Pt/YIG is essential for pursuing pure spin current phenomena, which rely heavily on Pt as a spin current generator or detector.

*clc@jhu.edu

[1] B. Heinrich, C. Burrowes, E. Montoya, B. Kardasz, E. Girt, Y.-Y. Song, Y. Sun, and M. Wu, Phys. Rev. Lett. **107**, 066604 (2011).

[2] S. O. Demokritov and A. N. Slavin, *Magnonics* (Springer Berlin, 2013).

[3] K.-i. Uchida, H. Adachi, T. Ota, H. Nakayama, S. Maekawa, and E. Saitoh, Appl. Phys. Lett. **97**, 172505 (2010).

[4] M. Weiler *et al.*, Phys. Rev. Lett. **108**, 106602 (2012).

[5] S. Y. Huang, X. Fan, D. Qu, Y. P. Chen, W. G. Wang, J. Wu, T. Y. Chen, J. Q. Xiao, and C. L. Chien, Phys. Rev. Lett. **109**, 107204 (2012).

[6] H. Nakayama *et al.*, Phys. Rev. Lett. **110**, 206601 (2013).

[7] Y. M. Lu, J. W. Cai, S. Y. Huang, D. Qu, B. F. Miao, and C. L. Chien, Phys. Rev. B **87**, 220409 (2013).

[8] C. Hahn, G. de Loubens, O. Klein, M. Viret, V. V. Naletov, and J. Ben Youssef, Phys. Rev. B **87**, 174417 (2013).

[9] M. Althammer *et al.*, Phys. Rev. B **87**, 224401 (2013).

[10] N. Vlietstra, J. Shan, V. Castel, B. J. van Wees, and J. Ben Youssef, Phys. Rev. B **87**, 184421 (2013).

[11] T. R. McGuire and R. I. Potter, IEEE Trans. Magn. **11**, 1018 (1975).

[12] R. C. O'Handley, *Modern Magnetic Materials: Principles and Applications* (Wiley, New York, 1999).

[13] Y.-T. Chen, S. Takahashi, H. Nakayama, M. Althammer, S. T. B. Goennenwein, E. Saitoh, and G. E. W. Bauer, Phys. Rev. B **87**, 144411 (2013).

[14] Y. Sun *et al.*, Phys. Rev. Lett. **111**, 106601 (2013).

[15] Y. M. Lu, Y. Choi, C. M. Ortega, X. M. Cheng, J. W. Cai, S. Y. Huang, L. Sun, and C. L. Chien, Phys. Rev. Lett. **110**, 147207 (2013).

[16] D. Qu, S. Y. Huang, J. Hu, R. Wu, and C. L. Chien, Phys. Rev. Lett. **110**, 067206 (2013).

[17] C. Burrowes, B. Heinrich, B. Kardasz, E. A. Montoya, E. Girt, Y. Sun, Y.-Y. Song, and M. Wu, Appl. Phys. Lett. **100**, 092403 (2012).

[18] B. F. Miao, S. Y. Huang, D. Qu, and C. L. Chien, Phys. Rev. Lett. **111**, 066602 (2013).

[19] T. Lin, C. Tang, and J. Shi, arXiv:1309.2213.

[20] W. J. Antel, Jr., M. M. Schwickert, T. Lin, W. L. O'Brien, and G. R. Harp, Phys. Rev. B **60**, 12933 (1999).

[21] S. Ruegg, G. Schutz, P. Fischer, R. Wienke, W. B. Zeper, and H. Ebert, J. Appl. Phys. **69**, 5655 (1991).

[22] F. Wilhelm *et al.*, Phys. Rev. Lett. **85**, 413 (2000).

[23] D. Qu, S. Y. Huang, B. F. Miao, S. X. Huang, and C. L. Chien, Phys. Rev. B **89**, 140407(R) (2014).

[24] W. E. Bailey, A. Ghosh, S. Auffret, E. Gautier, U. Ebels, F. Wilhelm, and A. Rogalev, Phys. Rev. B **86**, 144403 (2012).